

An Investigation of Gas-Powder Flow in Laser-Based Direct Metal Deposition

Srdja Zekovic, Rajeev Dwivedi, Radovan Kovacevic
Research Center for Advanced Manufacturing
Southern Methodist University, 1500 International Pkwy., Suite 100
Richardson, TX, 75081

Reviewed, accepted September 14, 2006

Abstract

Laser-Based Direct Metal Deposition (LBDMD) is a blown-powder laser deposition process which can produce fully-dense and metallurgically sound parts by a layered manufacturing method. Since a deposition head equipped with discontinuous radially symmetric nozzles has the potential to be tilted without influence of the gravity on the powder stream shape, it can be used for multi-axis deposition. The shape of the gas-powder stream with respect to the shape of laser beam and the size of the molten pool, have a large influence on the size and shape of the buildup. They determine the geometrical accuracy and the surface quality of the buildup. This paper examines gas-powder flow from radially symmetric nozzles using computational fluid dynamics method. For verification purpose the powder flow was investigated by a visualization method and powder concentration distribution was analyzed using image processing technique. The obtained results are in good agreement with numerical model.

1. Introduction

There are three different concepts of powder injection applied in direct laser metal deposition: off-axis powder injection (a single powder stream is fed laterally into the laser beam), continuous coaxial powder injection (a powder stream cone is produced that encloses the laser beam), and discontinuous coaxial powder injection (three or more powder streams are fed to the laser beam) (Fig. 1). The major advantage of the discontinuous coaxial powder injection is the potential to tilt the deposition head without influencing the powder stream. This feature allows multi-axis deposition [1].

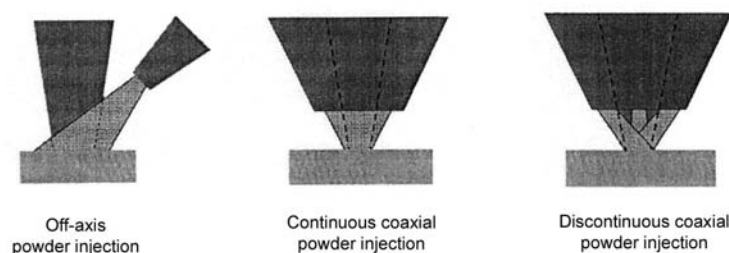


Fig. 1. Concepts of powder injection [1].

The MultiFab [2] system exploits the additive blown-powder LBDMD process for the near-net fabrication of fully-dense small and intricate features of metallic prototypes by a layered manufacturing method. Since the MultiFab is a multi-axis system, the discontinuous coaxial powder injection is the only appropriate concept. The MultiFab powder delivery subsystem consists of: an inert gas (Argon) source, powder feeders, and a nozzle setup on the laser head.

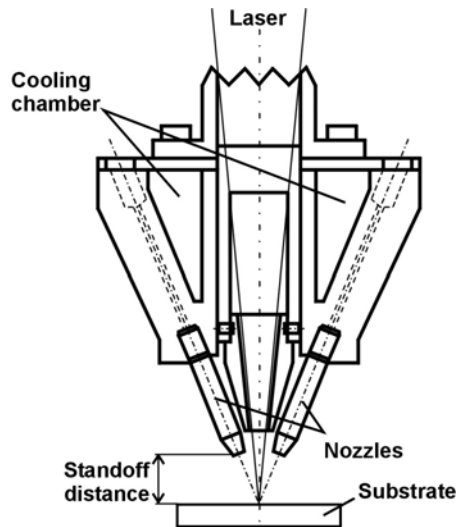


Fig. 2. Nozzle setup of powder delivery.

The nozzle's setup, as a part of the laser deposition head, is the key component of the powder delivery system. A proper nozzle design allows the cladding process to be completed in a single step. Fig. 2 shows the schematic and experimental nozzle setup applied in the powder delivery system. The deposition head provides the laser beam, powder, and protection gas. The Nd:YAG laser beam directed through the deposition head coaxial nozzle generates a molten pool in interaction with the metallic substrate. The powder, carried by the inert gas through four radially symmetrical nozzles at 30° to the vertical axis, is injected into the molten pool.

In addition to the set of the powder feeding nozzles, there is a coaxial nozzle in the center of the deposition head. The purpose of the coaxial nozzle, through which the laser beam is brought, is to direct an additional (secondary) inert gas stream toward the molten pool. The secondary stream is supposed to prevent the ricocheted particles and the fumes from the molten pool to reach and damage the optics for laser beam shaping in the deposition head.

The powder particles are injected from the feeding system through cylindrical inlets to the four powder feeding nozzles. Traveling along the nozzles, the particles collide with the nozzle walls. These collisions determine the concentration distribution and dispersion of the particles. After exiting the nozzles, the powder particles are drawn downward by the action of three factors: gravity, momentum from the transport gas, and momentum from the secondary gas flow. They then form one gas-powder stream directed to the molten pool.

The time and the spatial characteristics of the interaction between the powder and the laser beam are critical for the process. The physical properties of the powder material, the nature of the gas, the gas mass-flow rate, the stream spatial distribution, the particle size distribution, and the laser beam shape are among the parameters that are involved [3]. The shape of the gas-powder stream, combined with the size of the molten pool, have a large influence on the size and shape of the buildup, as well as on the powder efficiency; they determine the geometrical accuracy and the surface quality of the buildup. The shape of the gas-powder stream is tailored by the nozzle geometry: by the angle with respect to the vertical axis, by the vertical distance from the molten pool (or standoff distance), and by the gas velocity from the primary and secondary flows. Fearon et al. [4] investigated the effects of altering the configuration of a four-port nozzle system on the shape of the emitted powder streams. The possibility of depositing with a consistent layer height by controlling the powder efficiency in the vertical plane was demonstrated. As many operational parameters depend on the gas-powder stream characteristics between the nozzles and the deposition point, an extensive understanding of the powder stream properties, such as the concentration of the powder and the velocities of the gas and the powder particles will be helpful in determining the optimal operational parameters.

Given the complexity of the multiphase flow from a radially symmetric nozzle, it is difficult to model analytically, so a precise simulation of the flow structures is generally regarded as

requiring the numerical modeling technique [5]. Using a finite difference numerical algorithm based on a specific control-volume approach, the powder flow structures of a coaxial nozzle with various arrangements of the nozzle exit for laser cladding were simulated [6]. A 2-D axially symmetrical model of the two-phase turbulent gas-powder flow was used to investigate the influence of the nozzle arrangement and gas flow settings on the powder concentration in the stream. Also, a 2-D numerical discrete phase simulation was developed to study the effects of the coaxial nozzle converging angle and the gas settings (inner/outer gas stream relation) on the powder stream structure [7]. The particle path based on the coupled particle-gas interactions in the two-phase turbulent flow was predicted using stochastic tracking.

In order to simulate and study powder flow behavior involved in the MultiFab powder feeding system, a 3-D model of the turbulent gas-powder flow, based on the nozzle setup shown in Fig. 3.2, has been developed. FLUENT software, based on a finite-volume approach, is used to perform a detailed numerical analysis of the powder stream without laser radiation. Since the gas-powder flow is characterized by the turbulence, and turbulence in turn is a three-dimensional phenomenon, a 3-D model is required. The model is used to gain full insight into the process and to analyze the influence of the processing parameters such as the standoff distance, volumetric gas flow rate, and mass flow rate on the output of the LBDMD process. Also, the developed model provides important parameters for the calculation of the heat transfer boundary conditions for the finite element model (FEM) of the LBDMD process [8].

2. Numerical Study of the Gas and Powder Turbulent Flow

2.1 Turbulent Flow Modeling

A significant property of turbulent jet flow is that momentum, heat and mass are transferred across the flow at rates much greater than those of laminar flow with molecular transport processes by viscosity and diffusion. The numerical simulation of a turbulent flow involves modification of governing equations for case of laminar flow. For the flow involved in this study being steady, incompressible, isothermal, chemically homogeneous and without body forces the continuity and Navier-Stokes equations apply.

Following the original idea of Reynolds, we assume that the fluid is in a randomly unsteady turbulent state and work with the time averaged, or the mean equations of motion [9]. Therefore, turbulent modeling is the task of providing additional equations to describe the temporal and spatial evolution of the turbulent inertia flux. The most popular turbulence model in practical use is the so-called two-equation, or $k-\varepsilon$ model. In the $k-\varepsilon$ turbulent model the turbulence field is characterized by two variables, the turbulent kinetic energy k , and the viscous dissipation rate of turbulent kinetic energy ε .

2.2 Two-Phase Flow Modeling

As it is pointed out, the flow in the nozzles and in the first interaction zone between the nozzles and the substrate is not a simple one-phase turbulent flow. Instead, this flow can, at best, be approximated as a two-phase flow, where the primary phase is the inert gas, and the secondary phase consists of the powder particles mixed with the gas. Gas-particle flows are characterized by coupling between phases. The behavior of particles suspended in a turbulent flow depends on the properties of both the particles and the flow. The turbulent dispersion of

both the particles and the carrier gas can be handled by the concept of eddy diffusion energy in some range of the particle size distribution. The momentum transfer resulting from the interaction of the two phases has been investigated, and many criteria have been proposed. Because of the computation complexity of the particle and gas flow, many techniques have been proposed, but the uncertainty of the prediction model is still large [10-11].

In order to define the properties of a gas-particle mixture, the analyzed volume must be large enough to contain sufficient particles for a stationary average. A reasonable assumption is that the gas flow is responsible for the particle trajectories along the trajectories. This condition is identified as a one-way coupling [12-13]. The assumption of one-way coupling was used frequently in the early numerical and analytic models for gas-particle flows.

2.3 Dispersed Phase Modeling

In this study, the Lagrangian approach for two-phase flow modeling is used to model the powder particles mixing process. The underlying concept here is what is usually called dispersed two-phase flow. The idea is to consider one of the phases (powder particles) to be dispersed in the other phase (gas stream). At the same time, strong coupling occurs between phases. The Lagrangian model represents the dispersed phase as a continuous stream of particles moving through the carrier phase. The governing equations for the carrier phase are given in the standard fluid dynamics Eulerian frame of reference, while the motion of the particles is described in a Lagrangian coordinate system. The information transfer between phases is accounted for by the momentum along the particle paths. This two-way coupling is accomplished by alternatively solving the discrete and continuous phase equations until the solutions in both phases have stopped changing (i.e., until the convergence criteria are met).

2.4 Model Description

The solution technique used in this study is based on the FLUENT software that solves the conservation equations for mass and momentum by a specified finite-volume method [14]. The governing equations are discretized on a curvilinear grid to enable the computations in complex/irregular geometry.

The grid selection is important to improve the accuracy of the solutions in most numerical simulation methods. There are two methods of grid generation that can be adopted in FLUENT software. For a simple geometry without an edge or curve, the Cartesian coordinate grid system can be used. Otherwise, the body fitted coordinate (BFC) grid system is used. The acceptability of the grid generation is checked automatically by the FLUENT software and is verified using the residuals list of the convergence in the computation.

The computational domains are discretized using GAMBIT software. Since the geometry is complex, a non-conformal mesh must be used. Therefore, the segments of the computational domain such as the nozzles and the major parts of the cylindrical area below the nozzles can be meshed by hexagonal cells. From the other side, the part of the cylindrical area that is attached to the nozzles must be meshed by tetrahedral cells. To connect these zones, it is necessary to create interfaces between them. Fig. 3 shows the BFC grid selection for geometric domain in the gas-powder flow analyses.

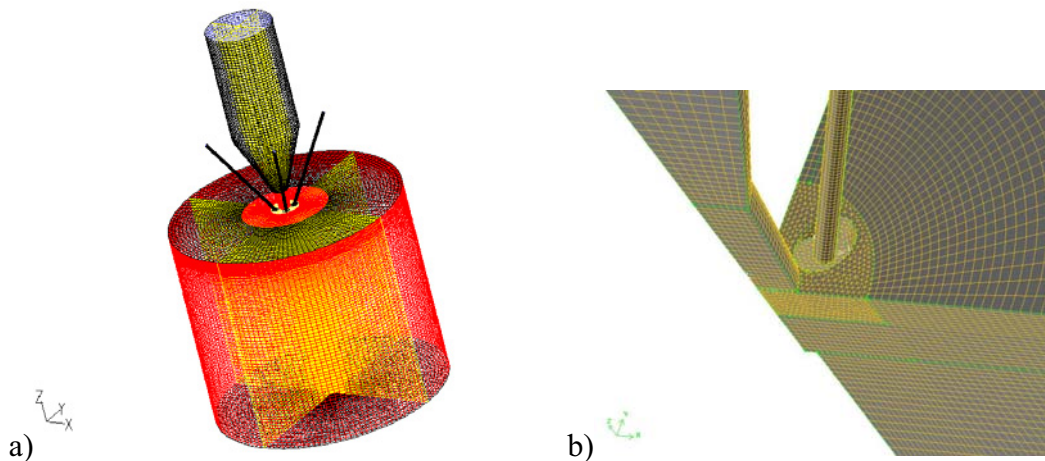


Fig. 3. Meshed geometry for flow analysis: a) free gas-powder flow, b) flow at detail at the nozzles' connecting zone.

The simulation of the jet flow by FLUENT software is performed under the following assumptions:

- The jet flow problem is treated as a steady-state turbulent flow with a constant velocity distribution in the inlet boundary.
- Drag force, inertia, and gravity are the only forces considered in this study; other forces such as pressure and the surrounding flow acceleration are neglected.
- Since the powder volume fraction in the flow is less than 10 % a dilute gas-particle stream is assumed. This assumption allows the application of one-way coupled discrete phase modeling.
- The effect of velocity fluctuation on a particle trajectory calculation is considered.
- The particle collision is not considered.
- The heat transfer by laser radiation is neglected.
- The particle size is assumed to follow the general Rossin-Rammler distribution expression [15].
- The molten pool is defined as a wall boundary condition with the ability to trap the particles. The pressure outlets ($p=0$) allow the particles to escape.

The solving procedure consists of the two steps: the turbulent steady state gas flow problem and discrete phase unsteady powder flow problem. In other words, the steady state gas flow is solved for the specific geometric domain, and after that particles are injected into the gas stream and followed during the time.

3. Powder Flow Visualization

The model of gas-powder flow that was previously introduced requires experimental verification. In order to investigate powder flow, digital imaging and analysis methods were selected, since they are non-intrusive and require no measuring equipment that could disturb the powder flow. Apparatus with a laser light source was used by Vetter, Engel and Fontaine [3] in a study of the laser cladding parameters. That work identified the position of phase changes in the powder, but did not explicitly measure powder concentrations, inferring the position of the

maximum concentration from power transmission along the axis. Meriaudeau et al. [16-17] made use of optical and image processing techniques to investigate the effect of the shroud gas flow on the powder beam width: although, this approach was considered along a single line at a fixed distance from the nozzle, so it did not allow an analysis of axial concentration variations. Similar techniques were proven effective for investigations into coaxial nozzle design [18], and powder stream concentration and catchment studies [19-22]. In these investigations, they were focused on the powder profile in the radial (transverse) direction, and powder concentrations were measured in a horizontal plane when a single powder stream was formed. The powder profile in the axial as well as the radial direction with the influence of the substrate position was investigated by Pinkerton et al. [23]. The visualization technique exploited the tungsten lamp as a light source, and image processing was used to measure the powder concentration in the vertical plane and horizontal plane. All these investigations were performed for the coaxial nozzles.

Fearon et al. [4] visualized powder a flow from radially symmetric nozzles. The method used was to direct a strong directional light source at the powder feed nozzle in operation, so that powder particles reflected this light toward a still camera. The resulting photographs were image processed in order to show clearly the resultant effects on the geometry of the powder cloud created by the intersection of the individual powder streams. They did not analyze the powder distribution in axial and radial direction of the powder cloud.

The method of image analysis used in this investigation is founded on the theory of the scattering of light by small particles (Mie theory) [24]. It is assumed that a powder cloud contains many scattering particles and is optically thin, so that the incident light intensity for each particle is the same. Then the reflected intensity is directly proportional to the particle density in the volume of powder cloud. Hence, the radiance of areas of the particle stream can be used as a direct measure of the density of reflective particles within it.

3.1 Experimental Procedure

The experimental apparatus used is illustrated in Fig. 4. This visualization technique was applied with a diode laser light source LasirisTM with a 660-nm wavelength. The laser beam passes through a structured light projector in order to provide a 200- μm thick sheet of light with uniform (non-gaussian) intensity distribution. The vertical sheet of light was projected through the powder cloud below the nozzle setup, and images were taken against a black background with a digital camera set to a high resolution (Fig. 4a). For horizontal cross sections of the powder cloud, the laser beam was projected horizontally, and the images were taken using a mirror set placed at 45° with respect to the horizontal plane (Fig. 4b). The light levels remained approximately constant throughout the experiment. For each picture an initial datum image was taken before powder flow was started. This datum image was subtracted from the final image, taken when the powder stream had become fully developed, prior to analysis.

The images of free powder flow were taken for a number of different set points characterized by different powder mass flow rates. The images were analyzed using the MATLAB software package. The pictures were scaled in terms of a pixel-to-mm ratio and the gray-level distributions along user-selected axes were extracted. The resulting data was exported in tabular form to Microsoft EXCEL spreadsheet software, the background measurements were subtracted, the values were normalized, and the results were graphed.

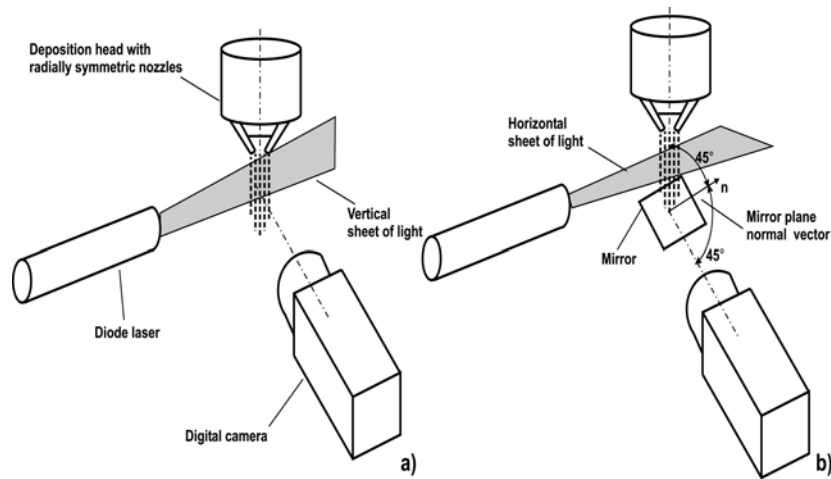


Fig. 4. Experimental setup for imaging of powder distribution in: a) vertical cross sections, and b) horizontal cross sections.

Table 1. Size distribution of H13 tool steel powder for the experiment [25].

U.S. standard mesh (powder size)	+80 ($>180\mu\text{m}$)	80/100 (180-150 μm)	100/140 (150-106 μm)	140/200 (106-75 μm)	200/270 (75-53 μm)	270/325 (53-45 μm)	325/D ($>45\mu\text{m}$)
Size analysis (%)	0	0.77	20.60	44.96	28.0	4.56	1.11

A H13 tool steel gas-atomized powder was used to perform experiments with the gas-powder flow. The size distribution of the powder particles of approximately spherical morphology is shown in Table 1. Carried by the primary inert gas flow $0.354 \text{ m}^3/\text{h}$, the powder particles travel through the four nozzles of the 0.9 mm diameter at a speed of 38.65 m/s . The powder mass flow rate as defined by powder feeder rotational speed is in the range $5 - 25 \text{ g/min}$ that represents less than 1% of the volumetric fraction in the stream. The secondary gas flows from the coaxial nozzle at a volumetric flow rate of $0.354 \text{ m}^3/\text{h}$. The standoff distance, in the case when the flow over the flat substrate or thin-walled structure was analyzed, measured from the top edge of the nozzle tips, was 4.75 mm .

4. Results and Discussion

The physical model of the compound jet with a dispersed powder was solved. The results are based on the different configurations in the three cases. Normally, more than 300 numerical iterations are required for the first step (gas flow) to be solved in each simulation case. To solve the coupling problem of the gas and powder phases, 300 iterations (time steps of 0.0001 s) were assigned. This time was long enough to follow the particles from the inlet to all domain boundaries.

The solution of the *free gas-powder flow* shows the turbulent nature in the area below the nozzles. The gas flow through the radially symmetric nozzles is transitional ($Re = 2000 \div 4000$); while in the area below the nozzles, it becomes turbulent.

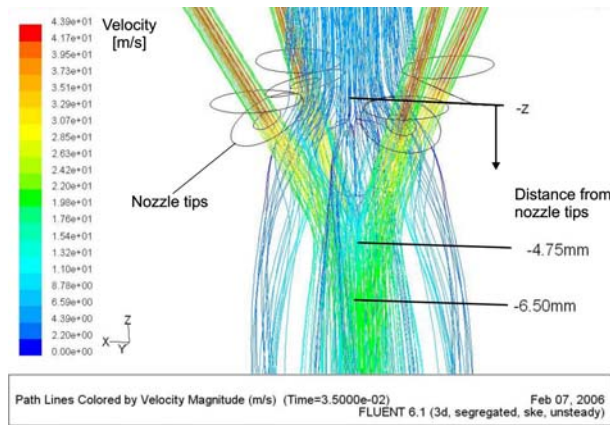


Fig. 5. Path lines of the gas free flow from the nozzles colored by velocity magnitude.

After leaving the nozzles, the four jets intersect with each other forming a cylindrical area of a maximum powder concentration along the vertical axis in the standoff distance range from -4.75 mm to -6.50 mm (Fig. 7). Fig. 7a shows a digital image of the powder cloud cross section below the nozzles where the pixel gray level corresponds to the powder concentration. Since the sheet of laser light projected through the cloud has a finite thickness of 200 μm , the image is slightly different from the concentration contours in the plane of symmetry (Fig. 7c), but it is in good agreement with the concentration contours in the plane 100 μm offset from the plane of symmetry.

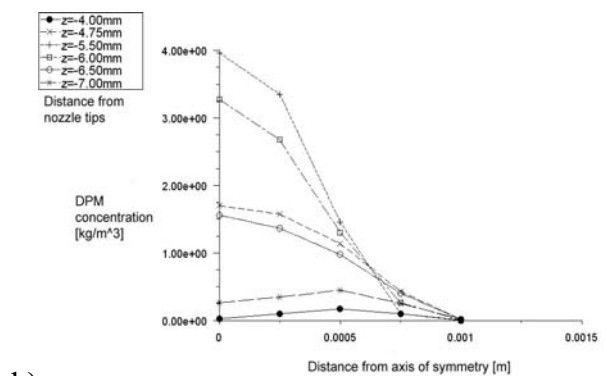
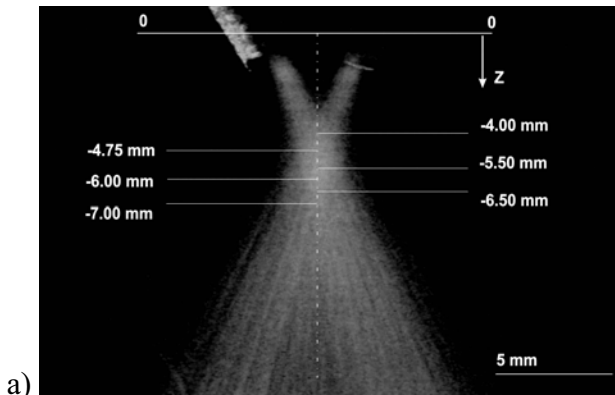


Fig. 6. a) Image of the powder flow, below the nozzles, b) Powder concentration variation in radial direction.

The curves of the powder concentration variation in the radial direction at different distances from the nozzle outlets are presented in Fig. 6b. They correspond to the different planes below the nozzles presented on the Fig. 6a. It is shown that the largest powder concentration is distributed along the axis of symmetry for the standoff distance from -4.75 to -6.50 mm.

A more detailed investigation of the powder concentration in the powder cloud in the axial and radial direction was performed. A simulation of the gas-powder flow for the range of processing parameters was performed. The influence of the powder mass flow rate and the powder volumetric flow rate (i.e. the particles speed) on powder concentration was analyzed.

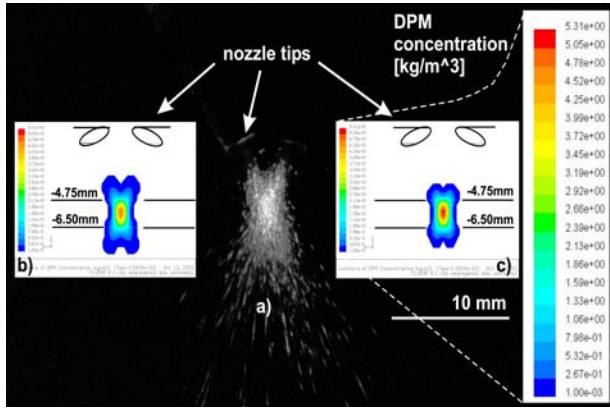


Fig. 7. Vertical cross section of powder cloud below the nozzles: a) digital image, b) concentration contours from simulation in the plane 100 μm offset from the plane of symmetry and c) concentration contours in the plane of symmetry.

The powder concentration variation in the axial direction versus the powder mass flow rate is displayed in Fig. 8a. The Fig. shows the location of the maximum concentration at the -5.50 mm position from the nozzle tips. As the powder flow increases the powder concentration increases, but the location of the maximum powder concentration in the axial direction does not change. Furthermore, the powder concentration was analyzed in the radial direction at the -5.50 mm axial distance from the nozzle tips. The powder concentration variation in the radial direction versus the powder mass flow rate is displayed in the Fig. 8b. It shows an increase of the powder concentration with an increase of the powder mass flow rate.

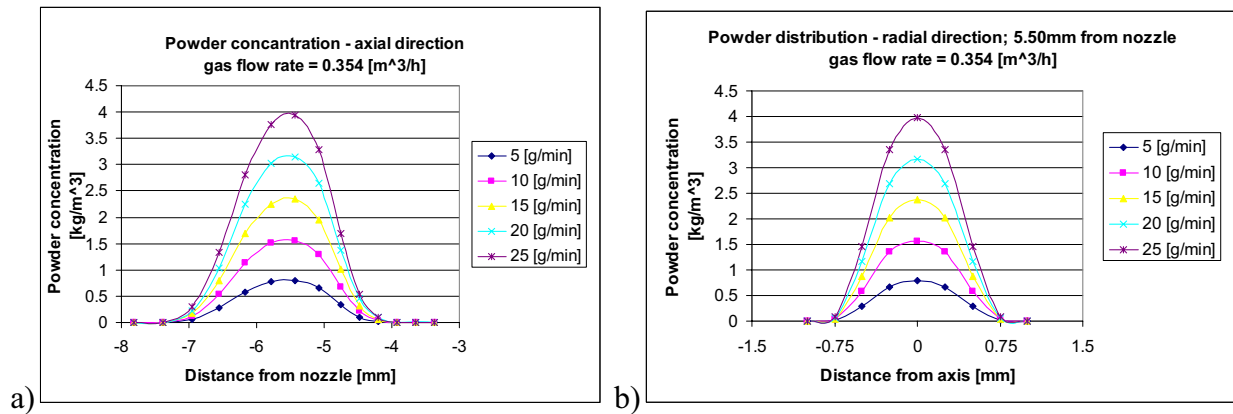


Fig. 8. Powder concentration distribution in at constant gas volumetric flow rate of $0.354 \text{ m}^3/\text{h}$ – model: a) axial direction, b) radial direction at -5.50mm.

To verify the results obtained from the numerical model, a visualization of the gas-powder flow was performed. The images of the powder cloud vertical cross sections through the axis are presented in the Table 2. Using the image processing powder concentration distribution along the vertical axis and in the radial direction at the -5.50 mm (shown in Table 2) location from the nozzle tips was analyzed. It should be noted that the scaling factor between the radiance and concentration, represented by the dimensionless function cannot be calculated directly; meaning that during the comparison of the measured radiance and concentration, the values from the model must usually be shown on different scales.

The powder concentration variation in the axial direction versus powder mass flow rate is displayed in Fig. 9a. It shows the location of the maximum concentration at the -5.50 mm location from the nozzle tips which is in agreement with the model. As the powder flow increases, the powder concentration increases, but the location of the maximum powder concentration in axial direction does not change.

Table 2. Powder distribution vs. powder flow in the vertical plane of symmetry.

Gas flow [m ³ /h]	Particle speed [m/s]	Powder flow [g/min]	Image
0.354	38.65	5	
0.354	38.65	10	
0.354	38.65	15	
0.354	38.65	20	
0.354	38.65	25	

As it was the case in the model, the powder concentration was analyzed in the radial direction at -5.50 mm axial position from the nozzle tips. The powder concentration variation in the radial direction versus powder mass flow rate is displayed in Fig. 9b. It shows an increase of the powder concentration with an increase of the powder mass flow rate.

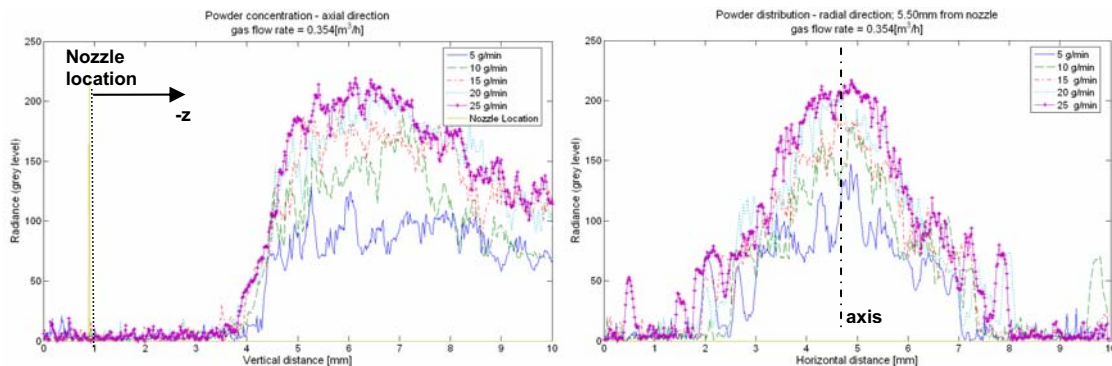


Fig. 9. Powder concentration distribution at constant gas volumetric flow rate of 0.354 m³/h – experiment: a) axial direction, b) radial direction at -5.50mm.

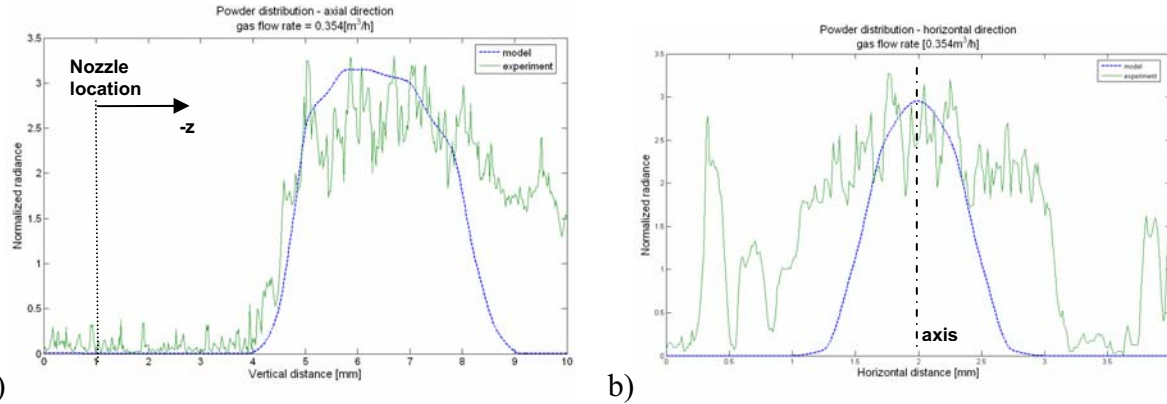


Fig. 10. Powder concentration distribution at constant powder mass flow rate of 15 g/min and particle speed of 38.64 m/s: model vs. experiment: a) axial direction, b) radial direction at -5.50mm.

Finally, the predicted (modeled) concentration variation results along the vertical axis are compared with those obtained experimentally for a representative set of the parameters (the powder mass flow rate is 15 g/min, and the particle speed is 38.65 m/s) in Fig. 10a. The two clearly show good agreement, both before and after the point at which the streams merge; although, the powder concentration far from the nozzle appears to be underestimated slightly. This underestimation may be attributed in part to the model not taking account of the particle collision, but may also be due to the scattered powder causing the experimental values to overestimate the concentration of nonrandom powder in this area. Fig. 10b shows good agreement in the location of the maximum powder density in the radial direction at the -5.50 mm axial position from the nozzle tips. The numerical results underestimate the width of the powder cloud since the model does not account for the particle collision.

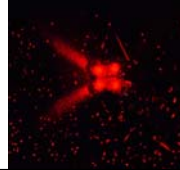
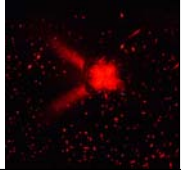
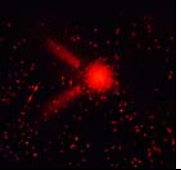
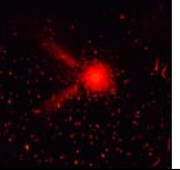
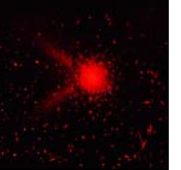
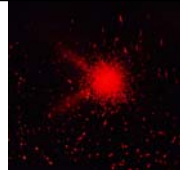
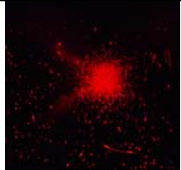
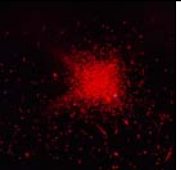
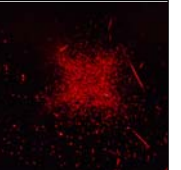
A better 3-D picture of the powder flow can be obtained displaying a set of horizontal cross sections of the powder cloud. Horizontal cross-sections of the powder flow streams from the model are presented in Fig. 11a. The set of images obtained by projecting a laser sheet through the powder cloud at different distances from the nozzle tips is presented in the Table 3. After image processing and arranging the images of the cross sections along the vertical axis, the 3-D shape of the powder flow is obtained (Fig. 11b). It shows good agreement with the corresponding results from the model (Fig. 11).

The comparison between the cloud images and numerically obtained powder concentration confirms the same location of the high powder concentration area. The analysis of the free flow shows that the standoff distance from 4.75 to 6.50 mm represents the limit that provides a coincidence of the powder cloud with the molten pool position for the best powder catchment efficiency. This zone is where the substrate or molten pool is supposed to be in order to provide a high quality deposition.

The comparison between the cloud images and numerically obtained powder concentration confirms the same location of the high powder concentration area. The analysis of the free flow shows that the standoff distance from 4.75 to 6.50 mm represents the limit that provides a coincidence of the powder cloud with the molten pool position for the best powder catchment

efficiency. This zone is where the substrate or molten pool is supposed to be in order to provide a high quality deposition.

Table 3. Images of the powder flow cross sections at specified distance from the nozzle tips.

				
-2.2 mm	-3.2 mm	-4.2 mm	-5.2 mm	-6.2 mm
				
-7.2 mm	-8.2 mm	-9.2 mm	-10.2 mm	-11.2 mm

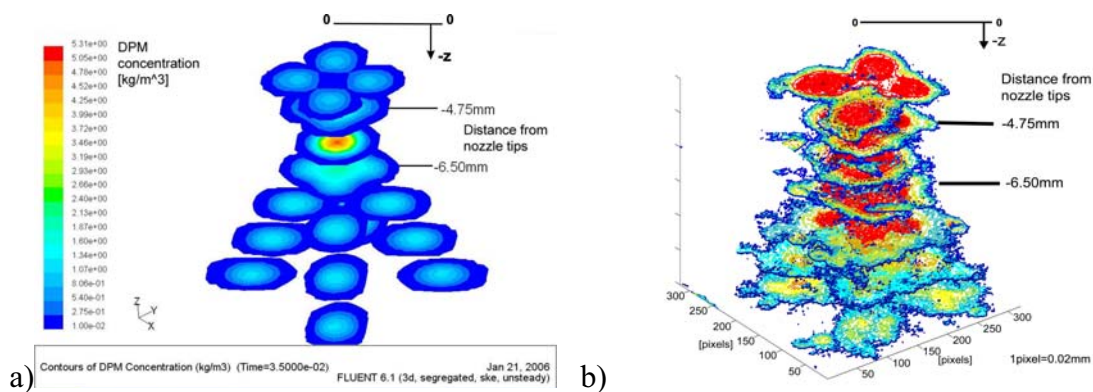


Fig. 11. Horizontal cross sections (powder concentration) of the powder streams: a) model, b) experiment.

According to the free gas-powder flow analysis, the standoff distance in the range from 4.75 mm to 6.50 mm can provide a high powder efficiency, as well as a stable deposition process that results in making an accurate buildup geometry. The verification of the numerical simulation results is performed by building the straight thin wall at different standoff distances. For the standoff distance between 4.75 mm and 6.50 mm, the wall is successfully built with an accurate height (Fig. 12a). The wall thickness is slightly varying as a consequence of the laser beam diameter variation with the change of standoff distance. During the experiments with a standoff distance less than 4.75 mm, the process becomes unstable because of the restricted powder delivery in the vertical plane. In this case, ripples on the top edge of the wall are formed. Furthermore, the laser beam becomes defocused along the top edge of the wall, and the geometrical error propagates as the deposition continues. In this case, the required wall geometry is not achieved (Fig. 12b). This result is in good agreement with the results from Fearon et al. [4], where they investigated the influence of the powder stream geometry on the process stability and the deposited layer height.

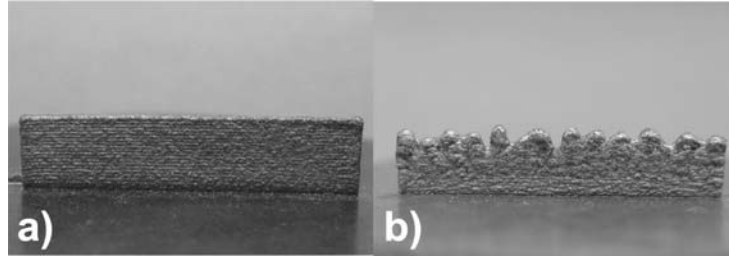


Fig. 12. Buildup geometry deposited with a) standoff distance from 4.75 mm to 6.50 mm, and b) with standoff distance less than 4.75 mm.

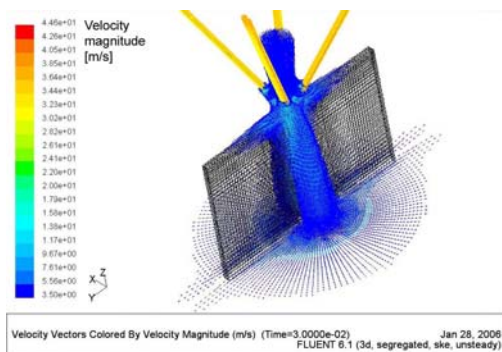


Fig. 13. Gas velocity vectors around the wall.

The model of gas-powder flow around the wall was developed as a complementary model to the thermo-structural FEM of the LBDMD of thin-walled structures [8]. The distribution of the gas velocity around the wall was used to calculate the correct boundary conditions for the heat transfer model. The model reveals zones of intense gas flow over the wall surfaces (Fig. 13). These areas are exposed to forced convection, and the coefficient of heat transfer between the wall and the surrounding area can be calculated using the gas velocity values obtained from the gas flow analysis.

5. Conclusions

The results discussed in this chapter seek to address some powder delivery issues associated with the laser-based direct metal deposition. The potential of the process of numerical modeling combined with the experimental results is used as a powerful tool to obtain a better understanding of the phenomena observed during the direct laser metal deposition, and to analyze the influence of the gas-powder flow characteristics on the process stability and the process output. A 3-D discrete phase model of the gas-powder flow in the LBDMD process was developed using FLUENT numerical software.

The significant findings derived from this work are summarized below:

1. Since the particle volume fraction of the powder in the gas flow is less than 10%, a discrete phase model is used to simulate the process.
2. The powder flow pattern after the nozzle outlet is slightly different from the gas flow. The powder concentration distribution reveals that the standoff distance in a specific range can provide a stable powder delivery and accurate buildup geometry, which is in agreement with the experimental results.
3. The numerical model of gas-powder flow shows its robustness, giving good results for a variety of input parameters and can be used for nozzles geometry optimization.
4. The gas flow model around the wall, as a complementary model to the thermo-structural FEM of laser metal deposition, provides important data for the calculations of the boundary conditions in the heat transfer model.

Acknowledgements

This work was financially supported by the National Science Foundation Grants No. DMI-0320663 and No. DMI-0541952. The authors would like to acknowledge Mr. Michael Valant, research engineer at the Research Center for Advanced Manufacturing, Southern Methodist University, for his contribution in the experimental part of this work.

REFERENCES

- [1] A., Weisheit, G., Backes, R., Stromeyer, A., Gasser, K., Wissenbach, R., Poprawe, 2001, "Powder Injection: The Key to Reconditioning and Generating Components Using Laser Cladding, Proceedings of International Congress on Advanced Materials and Processes, Materials Week 2001, Munich, Germany.
- [2] Kovacevic, R., Valant, M., 2006, System and Method for Fabrication or Repairing Part, US Patent No. 7,020,539.
- [3] Vetter, P.A., Engel, Th., and Fontaine, J., 1994, "Laser Cladding: The Relevant Parameters for Process Control," SPIE Vol. 2207, pp.452-462.
- [4] Fearon, E., Watkins, K.G., 2004, "Optimization of layer height control in direct laser deposition," Proceedings of the 23rd International Congress on Applications of Laser and Electro-optics (ICALEO 2004), San Francisco, CA.
- [5] Levy, S., 2000, "Two-Phase Flow in Complex Systems," John Wiley & Sons Inc., New York.
- [6] Lin, J., 2000, "Numerical simulation of the focused powder streams in coaxial laser cladding," Journal of Materials Processing Technology, Vol. 105, pp. 17-23.
- [7] Liou, F.W., Ruan, J., Pan, H., Han, L., and Boddu, M.R., 2004, "A Multi-Axis Hybrid Manufacturing Process," 2004 NSF Design, Service and Manufacturing Grantees and Research Conference/SMU, Dallas, Texas.
- [8] Zekovic, S., Dwivedi, D., and Kovacevic, R., 2005, "Thermo-structural Finite Element Analysis of Direct Laser Metal Deposited Thin-Walled Structures," Proceedings of Solid Freeform Fabrication Symposium, Austin, Texas.
- [9] Rajaratnam, N., 1976, "Turbulent jets," Elsevier, Amsterdam.
- [10] Antonia R.A., and Bilger, R.W., 1973, "An experimental investigation of an axisymmetric jet in co-flowing air stream," Journal of Fluid Mechanics, Vol.61, pp.805-822.
- [11] Streeter, V.L., 1961, "Handbook of Fluid Dynamics," McGraw-Hill, New York.
- [12] Crowe C.T., 1982, "Review – numerical models for dilute gas-particle flows," ASME Transactions, Journal of Fluid Engineering, Vol.104, pp.297-303.
- [13] Sharma M.P., and Crowe, C.T., 1978, "A novel physico-computational model for quasi one-dimensional gas-particle flows," ASME Transactions, Journal of Fluid Engineering, Vol.100, pp. 343-349.
- [14] Fluent Inc., 2004, "FLUENT 6.2.1 User Guide," USA.
- [15] Fan, J., Zhao, H., and Chen, K., 1992, "An experimental study of two-phase turbulent coaxial jets," Experiments in Fluids, 13, pp. 279-287.
- [16] Meriaudeau, F., and Truchete, F., 1996, "Control and Optimization of the Laser Cladding Process Using Matrix Cameras and Image Processing," Journal of Laser Applications, 8, pp. 317-324.

- [17] Meriaudeau, F., Truchetet, F., Grevey, D., and Vannes, A.B., 1997, "Laser Cladding Process and Image Processing," *Lasers in Engineering*, 6, pp. 161-187.
- [18] Lin, J., and Steen, W. M., 1998, "Design Characteristics and Development of a Nozzle for Coaxial Laser Cladding," *Journal of Laser Applications*, 10(2), pp. 55-63.
- [19] Lin, J., 2000, "Laser Attenuation of the Focused Powder Streams in Coaxial Laser Cladding," *Journal of Laser Applications*, 12(1), pp. 28-33.
- [20] Lin, J., and Steen, W. M., 1997, "Powder Flow and Catchment During Coaxial Laser Cladding," *Proc. SPIE*, 3097, pp. 517-528.
- [21] Lin, J., 1999, "Concentration Mode of the Powder Stream in Coaxial Laser Cladding," *Optics & Laser Technology*, 31(3), pp. 251-257.
- [22] Lin, J., and Hwang, B.C, 1999, "Coaxial Laser Cladding on an Inclined Substrate," *Optics & Laser Technology*, 31(8), pp. 571-578.
- [23] Pinkerton, A.J., Lin, L., 2004, "Modeling powder concentration distribution from a coaxial deposition nozzle for laser-based rapid tooling," *Journal of Manufacturing Science and Engineering*, ASME 126, pp. 28-33.
- [24] Van de Hulst, H.C., 1957, "Light Scattering By Small Particles," General Publishing Co, Toronto.
- [25] Choi, J., and Hua, Y., 2004, "Dimensional and material characteristics of direct deposited H13 tool steel by CO₂ laser," *Journal of Laser Applications*, 16(4), pp. 245-251.